Incommensurate-to-incommensurate phase transition in Eu metal at high pressures

R. J. Husband,[1] I. Loa,[1] K. A. Munro,[1] E. E. McBride,[1,*] S. R. Evans,[3] H.-P. Liermann,[2] and M. I. McMahon[1,4]

[1]*SUPA, School of Physics and Astronomy and Centre for Science at Extreme Conditions, The University of Edinburgh, Mayfield Road, Edinburgh, EH9 3JZ, United Kingdom*

[2]*Photon Sciences, Deutsches Elektronen Synchrotron (DESY), Notkestrasse 85, D-22607 Hamburg, Germany*

[3]*European Synchrotron Radiation Facility, 38043 Grenoble, France*

[4]*Research Complex at Harwell, Didcot, Oxon, OX11 0FA, United Kingdom*

(Received 11 September 2014; revised manuscript received 5 November 2014; published 8 December 2014)

High pressure x-ray powder-diffraction experiments were performed on europium metal up to ∼70 GPa. Above 38 GPa, europium transforms from the incommensurately modulated Eu-IV phase to a second phase with an incommensurately modulated crystal structure, Eu-V. This is a previously unseen incommensurately modulated to incommensurately modulated transition in the elements at high pressure. High-pressure high-temperature experiments were also performed up to 449 K in order to make an initial estimate of the positions of the phase boundaries of the incommensurate phases.

DOI: 10.1103/PhysRevB.90.214105 PACS number(s): 61.50.Ks, 62.50.−p

I. INTRODUCTION

Europium (Eu), which is divalent at ambient pressure due to its half-filled $4f$ electron shell, is an anomalous member of the lanthanide elements, the majority of which are trivalent. Consequently, Eu does not exhibit the common series of structural phase transitions observed in the trivalent lanthanide elements on compression (hcp–Sm-type–dhcp–fcc–distorted-fcc–low-symmetry phase) [1], but instead its behavior is much more complex.

Eu transforms from the ambient-pressure body-centred cubic (bcc) structure to the hexagonal close-packed (hcp) structure at 12.5 GPa. Initial high-pressure x-ray diffraction studies [2–5] reported a transition to a new phase Eu-III above 17 GPa. This was identified by the appearance of a number of weak reflections in the diffraction pattern in addition to those from the hcp phase. However, we have shown that if great care is taken to minimize any possible sources of contamination during the preparation and pressure cell loading process, no additional peaks are observed above 17 GPa, and instead Eu remains in the hcp phase up to 31.5 GPa [6]. We therefore concluded that the behavior initially attributed to a transition to Eu-III was not due to changes in Eu itself, but was instead due to pressure-induced changes in a contaminant phase that was present in previous studies.

The presence of this contaminant phase in early x-ray diffraction studies greatly complicated the analysis of data collected above 17 GPa. Collecting diffraction data on non-contaminated samples allowed us to determine a transition to a new phase, Eu-IV, above 31.5 GPa [7]. The diffraction patterns from this phase are complex, and high-resolution diffraction data were required in order to resolve the large number of closely spaced reflections, and to identify the large number of weak reflections that appear at the transition. This enabled us to unambiguously determine Eu-IV to have an incommensurately modulated crystal structure (denoted i-$mC4$ in Pearson's notation, where i indicates that the structure is incommensurate and $mC4$ is the Pearson symbol for the average structure) [7]. This structure has a modulation vector in the a-c plane (q_1, 0, q_3), with superspace group $C2/c(q_1 0 q_3)00$ and atoms in the (0, y, 0.25) Wyckoff positions. We found that the i-$mC4$ structure can describe all of the diffraction patterns of Eu collected between 31.5 and 37 GPa, the highest pressure reached in our previous study. Eu-IV is currently the only incommensurate crystal structure to have been observed in the lanthanide elements at high pressure.

In our subsequent study [8], further changes were observed in the diffraction patterns of Eu collected above 38 GPa and we found that these patterns could no longer be described by the i-$mC4$ structure. This was taken as evidence of a transition to a new phase Eu-V, which was thought to be incommensurate, although we were unable to determine the structure at that time.

Despite the fact that europium exhibits possibly the most interesting high-pressure phases of any lanthanide element, there have been surprisingly few studies on its high-pressure behavior. With the exception of our earlier work [8], only one previous study has reported the results of x-ray diffraction experiments on Eu at pressures greater than 40 GPa. Bi *et al.* [5] reported a series of phase transitions and structural assignments in Eu up to 92 GPa. However, reflections from the contaminant phase can clearly be identified in their diffraction profiles collected above 18 GPa. Consequently, we found that none of the structures proposed by Bi *et al.* could describe our own data collected at pressures exceeding 18 GPa.

In this paper we report the results of powder x-ray diffraction experiments on Eu up to ∼70 GPa. We show that Eu transforms from i-$mC4$ to a second incommensurately modulated crystal structure Eu-V above 38 GPa. This transition is an example of an incommensurate-to-incommensurate transition in a non-host-guest structure, previously unseen in the elements at high pressure. The diffraction patterns from Eu-V are complex, and high-quality data are required in order to resolve the large number of closely spaced diffraction peaks. Significant peak broadening was observed in the diffraction profiles collected above ∼40 GPa, making it increasingly more difficult to analyze the patterns above this pressure.

We also report the results of our high-pressure high-temperature experiments up to ∼450 K and 42 GPa, in an

*Present address: Photon Sciences, Deutsches Elektronen Synchrotron (DESY), Notkestrasse 85, D-22607 Hamburg, Germany.

initial attempt to expand the phase diagram of Eu away from only room temperature studies. We find that the pressure range in which the hcp phase is stable is larger than in our room temperature experiments, with the hcp phase remaining stable up to higher pressures.

II. EXPERIMENTAL DETAILS

High-purity Eu samples, provided by U. Schwarz of the MPI für Chemische Physik fester Stoffe, were loaded into diamond-anvil cells equipped with tungsten or rhenium gaskets in a dry argon environment. Initial room temperature studies were performed on two samples, one of which was loaded without a pressure-transmitting medium (PTM), whereas the other was loaded with a helium PTM. In both of these samples, a small ruby sphere was included as a pressure marker, and the pressure was determined with the ruby fluorescence method using the calibration by Mao *et al.* [9].

Eu is extremely reactive, and great care must be taken in the loading procedure in order to minimize any possible sources of contamination. Reflections of the most common contaminant phase are not observed at pressures below 17 GPa, and so single-phase hcp Eu patterns must be collected in the 17–31.5 GPa region in order to confirm that the sample is "clean" [6]. We previously found that loading samples quickly without a PTM and without a pressure marker was the most effective way of obtaining noncontaminated samples [6,7]. The majority of the room-temperature data were therefore collected from a third sample loaded according to this method. The pressure of this sample was subsequently determined from the position of one or more sample reflections using a calibration established from the sample loaded in He and with a ruby pressure marker.

Two additional Eu samples were loaded in cells equipped with W gaskets for the high-temperature experiments. In one of these samples, a small grain of Ta powder was included as a pressure marker, and in the other sample a piece of 1 μm thick Ta foil was placed between the sample and one of the diamond anvils. The pressures of both samples were determined using the ambient-temperature pressure-volume relation of Ta measured by Hanfland *et al.* [10,11], and a thermal correction based on the results of Dorogokupets and Oganov [12] was applied for the high-temperature experiments. The cells containing these samples were heated using external resistive heaters, and the temperature was measured using a K-type thermocouple placed on the back of one of the diamonds. The uncertainty in temperature was estimated to be no more than 10 K.

Angle-dispersive powder x-ray diffraction data were collected on station ID09a at the European Synchrotron Radiation Facility (ESRF) and on beamline I15 at Diamond Light Source (DLS), using monochromatic x-ray beams of wavelength $\sim$0.41 and $\sim$0.34 Å and with diameters of 10 and 30 μm, respectively. Data were collected using a mar555 area detector (ID09a) and a mar345 image plate detector (I15). Additional data were collected on the Extreme Conditions Beamline (P02.2) at the PETRA III synchrotron, DESY, using an x-ray beam of wavelength $\sim$0.29 Å focused to $\sim 2 \times 2$ μm^2. Data were collected at Petra-III using an Perkin Elmer XRD 1621 area detector. In all cases, the 2D diffraction images were integrated using Fit2D [13,14] to produce 1D diffraction profiles, which were then indexed using the DICVOL [15] and SUPERCELL [16] indexing programs, and subsequently analyzed using the Le Bail and Rietveld methods with the JANA2006 software [17].

III. RESULTS

A. Transition to Eu-V

In all of our samples we observed the bcc–hcp transition in agreement with previous studies [2–7], and Eu transformed to the incommensurately modulated i-$mC4$ structure at 31.5 GPa. Preliminary studies performed on station ID09a found that although the i-$mC4$ structure gives an excellent fit to the diffraction profiles collected in the 31.5–38 GPa region, it could not explain the patterns collected at higher pressures. This suggested a transition to a new crystal structure above 38 GPa. This behavior was observed in both the sample loaded with a He pressure-transmitting medium and a sample loaded without a PTM.

Initial attempts to index this new phase were unsuccessful. However, analysis of data from these samples was complicated by the presence of contaminant reflections, the details of which have been reported previously [6,8]. The diffraction profiles from Eu above 31.5 GPa are extremely complex, and great care must be taken in order to find a unique structural solution for the new phases. It was therefore essential to collect data on noncontaminated samples to avoid misidentification of contaminant peaks as those from pure Eu, particularly as the behavior of the contaminant phase has only been established up to 38 GPa [8].

We therefore loaded a sample without a pressure marker and without a PTM with the aim of obtaining a noncontaminated sample. Data from this sample were collected on beam line I15 up to a maximum pressure of 46 GPa, the highest pressure that could be reached with the pressure cell. In this sample we did not observe the appearance of any contaminant reflections above 17 GPa, and instead Eu remained in the hcp phase up to 31.5 GPa. Above this pressure, data were collected in $\sim$1 GPa steps so that subtle changes in the diffraction patterns could be identified. The i-$mC4$ structure gives an excellent fit to the diffraction patterns collected in the 31.5–38 GPa region. The highest-pressure single-phase i-$mC4$ pattern at 38 GPa is shown in Fig. 1. The Bragg reflections can be indexed using four Miller indices (h,k,l,m) according to $\mathbf{H} = h\mathbf{a}^* + k\mathbf{b}^* + l\mathbf{c}^* + m\mathbf{q}$, where $\mathbf{a}^*,\mathbf{b}^*,\mathbf{c}^*$ define the reciprocal lattice of the $mC4$ average structure and $\mathbf{q}$ is the modulation vector, according to the 4D superspace formalism [18] as described in our previous work [7,19]. Only first-order ($m = \pm 1$) satellite reflections were observed. In our previous work we described the i-$mC4$ structure in the $C2/c(q_1 0 q_3)00$ superspace group setting in order to allow a direct comparison with the hcp structure in the orthohexagonal setting, and so the same superspace group will be used here. A Rietveld refinement of the i-$mC4$ structure based on the diffraction profile of Eu at 38 GPa gives lattice parameters of $a = 3.0508(4)$ Å, $b = 5.2196(4)$ Å, $c = 4.6524(4)$ Å, and $\beta = 90.541(9)^\circ$, and the atomic coordinate $y = 0.3264(9)$, with wave vector components $q_1 = 0.7684(5)$ and $q_3 = 0.5864(4)$ and modulation amplitudes of $B_{1a} = -0.048(4)$, $A_{1b} = 0.0292(15)$, and $B_{1c} = 0.0557(14)$. All other first-order Fourier components are equal to zero due to the superspace group symmetry conditions. These are

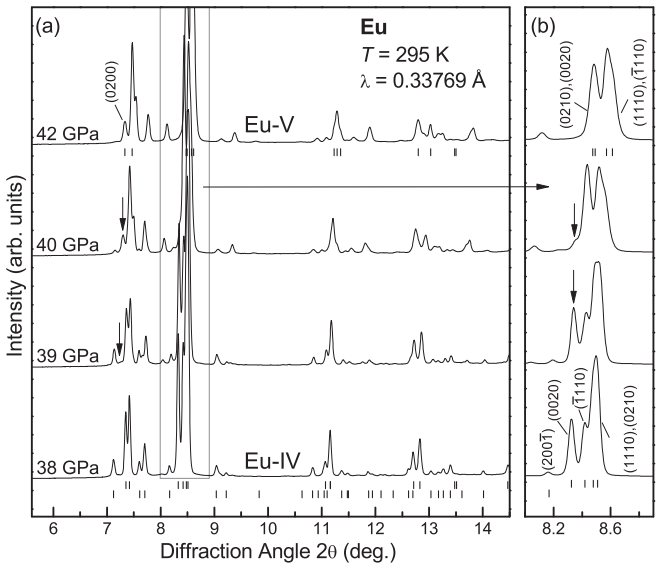

FIG. 1. (a) X-ray powder diffraction profiles of Eu at 38, 39, 40, and 42 GPa illustrating the transition from Eu-IV to Eu-V. The 38 GPa profile can be indexed as single-phase Eu-IV, the 39 and 40 GPa profiles are mixed-phase, and the 42 GPa profile is single-phase Eu-V. The upper and lower tick marks below the 38 GPa pattern indicate the calculated peak positions of the main and satellite reflections from i-$mC4$, respectively, and the tick marks below the 42 GPa pattern indicate the positions of $mC4(2)$, the average structure of Eu-IV. The arrows indicate the growth of the (0200) $mC4(2)$ reflection. (b) Enlargement showing the behavior of the (0020), ($\bar{1}110$), (1110), and (0210) i-$mC4$ reflections across the transition. The arrows indicates the disappearance of the (0020) i-$mC4$ reflection. The indices above the 42 GPa profile correspond to describing the $mC4(2)$ structure in the $\beta < 90^\circ$ setting.

in agreement with the structural parameters we previously determined for the i-$mC4$ structure [7].

Above 38 GPa we observed changes in the diffraction profiles which meant that they could no longer be described by the i-$mC4$ structure. This was taken as evidence of a transition to a new phase Eu-V, which was complete by 42 GPa. This is illustrated in Fig. 1(a), which shows diffraction patterns from Eu in the Eu-IV phase at 38 GPa, in the mixed-phase region at 39 and 40 GPa, and in the Eu-V phase at 42 GPa. The changes in the diffraction profiles during the transition can be characterized by three distinct features. First, we observed the appearance of a set of new reflections that cannot be accounted for by the i-$mC4$ structure. Second, the intensity of the i-$mC4$ satellite reflections began to decrease until they had completely disappeared by 42 GPa. Finally, subtle changes in the main i-$mC4$ reflections were also observed. In particular, the intense (0020) main reflection was observed to decrease in intensity until it had completely disappeared by 42 GPa, as illustrated in Fig. 1(b).

Additional data from this sample were collected on beamline P02.2 and in a second experimental run on I15, where the pressure was first decreased in order to observe the transition back into the Eu-IV phase, and then increased again to transform back into the Eu-V phase. In this case we observed the Eu-IV–EuV transition at a slightly lower pressure, and the lowest-pressure single-phase Eu-V pattern was collected at 40.3 GPa. These additional data sets were considered alongside the original data collected on I15 during the process of indexing the patterns from the new phase.

Attempts to index all of the reflections from Eu-V based on a crystal structure with a 3D space group were unsuccessful. However, as we noted previously [8], the fact that the overall diffraction profile of the new phase is very similar to that of Eu-IV suggested the possibility that Eu had transformed to a second incommensurately modulated crystal structure. In addition, a large number of weak reflections appear at the transition to Eu-V, which may be a new set of satellite reflections.

In order to index the Eu-V patterns based on an incommensurately modulated crystal structure, it is necessary to identify the main diffraction peaks so as to determine the average structure. However, although there is clear distinction between main ($m = 0$) and satellite ($m \neq 0$) reflections in the diffraction patterns from the Eu-IV phase, the reflections in the Eu-V patterns could not be distinguished with the same certainty. The main i-$mC4$ reflections in Eu-IV can be identified by two distinct features. First, they are much more intense than the surrounding satellite reflections. Second, they result from a continuous splitting of the hcp reflections as Eu transforms from hcp Eu-II to the lower-symmetry monoclinic Eu-IV structure. However, these features are not so easily identifiable in the Eu-V patterns. The positions of some of the main i-$mC4$ reflections can be clearly identified over the course of the transition, and we therefore assumed these also to correspond to main reflections of the new phase. As noted previously, at least one of the main i-$mC4$ reflections, (0020), disappears at the transition, suggesting that there is a change in the average structure. In addition, some of the new reflections that appear at the transition have an intensity comparable to that of the main Eu-IV reflections, and it is not immediately obvious if these are main or satellite reflections from the new phase.

However, the changes in the main i-$mC4$ reflections at the transition to Eu-V are subtle, and so we made the initial assumption that the average structures of both phases are similar. The DICVOL program was therefore used to index a subset of the reflections based on a similar monoclinic unit cell, ensuring that all of the reflections previously identified as main Eu-V reflections were accounted for. The best fit was obtained using a monoclinic structure with space group $C2/c$ with the atoms in the 4e (0, y, 0.25) Wyckoff positions. We denote the average structure as $mC4(2)$, where the 2 distinguishes it from the average Eu-IV structure, $mC4$. Please note that although both the $mC4$ and $mC4(2)$ structures have the $C2/c$ space group, they are not related to the $C2/c$ structure proposed by Bi *et al.*. A Rietveld refinement of this structure at 42 GPa gives lattice parameters of $a = 2.9756(18)$ Å, $b = 5.278(6)$ Å, $c = 4.564(4)$ Å, and $\beta = 89.66(7)^\circ$, with the atomic coordinate $y = 0.337(5)$. The positions of the main $mC4(2)$ reflections are shown by the tick marks under the diffraction profile of Eu at 42 GPa in Fig. 1. This structure can account for the set of reflections originally identified as the main Eu-IV reflections, and also at least one of the new reflections that appeared at the transition. This is illustrated in Fig. 1(a), which shows the growth of the (0200) reflection, which cannot be related to any of the peaks in the Eu-IV pattern.

The program SUPERCELL was then used to index the remaining reflections as satellite reflections corresponding to

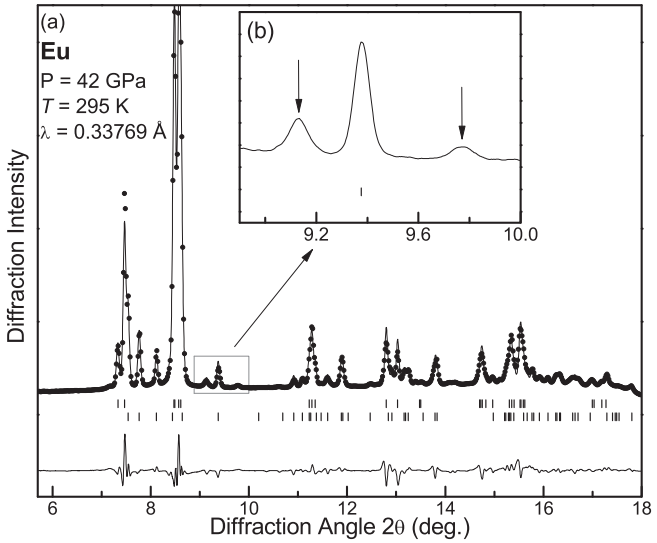

FIG. 2. Rietveld refinement of the i-$mC4(2)$ structure based on the diffraction profile of Eu at 42 GPa, where only first order ($m = \pm 1$) satellite reflections have been considered. (a) The points show the experimental data, and the solid line shows the fit. The tick marks below the profile show the calculated peak positions of the main (upper) and satellite (lower) reflections, and the residuals are shown below the tick marks. Inset (b) illustrates the most intense reflections that cannot be accounted for by main or first-order satellite reflections, which are indicated by the arrows above the profile. In this case, the solid line shows the experimental data.

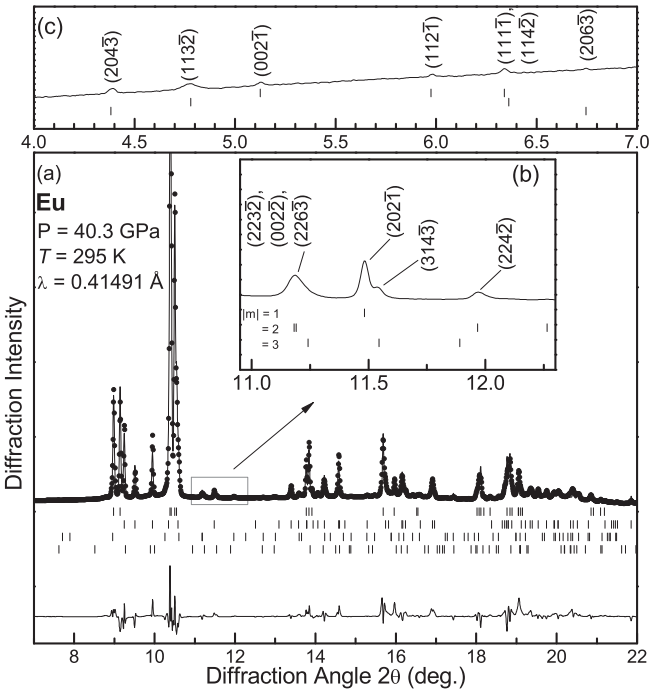

FIG. 3. Rietveld refinement of the i-$mC4(2)$ structure based on the diffraction profile of Eu obtained at 40.3 GPa, where up to third-order ($m = \pm 3$) satellite reflections have been considered. The points show the experimental data, and the solid line shows the fit. The tick marks below the profile show the calculated peak positions of the main (upper) and satellite (lower) reflections, and the residuals are shown below the tick marks. Inset (b) illustrates weak reflections that cannot be described as main or first-order satellite reflections, but can be accounted for when up to third-order satellite reflections are considered. Inset (c) illustrates a number of extremely weak low-angle satellite reflections that can be described by this structure. In insets (b) and (c), the solid line shows the experimental data. The indices correspond to describing the structure with $\beta > 90^\circ$.

a modulation wave vector (q_1,0,q_3), with $q_1 \approx 0.6$ and $q_3 \approx 0.4$. Analysis of systematic absences showed the superspace group to be $C2/c(q_1 0 q_3)00$ [i-$mC4(2)$, where again the (2) distinguishes this from the Eu-IV i-$mC4$ structure]. The i-$mC4$ and i-$mC4(2)$ structures therefore have the same superspace groups, with very similar lattice parameters, but with different modulation vectors. However, we described i-$mC4$ with $\beta > 90^\circ$ and i-$mC4(2)$ with $\beta < 90^\circ$. In order to compare the two structures, it is necessary to also describe i-$mC4(2)$ with $\beta > 90^\circ$. This involves the transformations $\beta' = 180^\circ - \beta$ and $q_3' = 2 - q_3$. The i-$mC4(2)$ structure will be described in this setting from now on. A Rietveld refinement of the i-$mC4(2)$ structure at 42 GPa is shown in Fig. 2, where only first-order ($m = \pm 1$) satellite reflections have been considered. The refined structural parameters are $a = 2.9761(3)$ Å, $b = 5.2809(7)$ Å, $c = 4.5613(6)$ Å, $\beta' = 90.372(10)^\circ$, and the atomic coordinate $y = 0.3371(9)$, with wave vector components $q_1 = 0.5869(3)$ and $q_3' = 1.5877(4)$ and modulation amplitudes of $B_{1a} = 0.061(3)$, $A_{1b} = -0.041(2)$, and $B_{1c} = 0.0667(15)$. As with Eu-IV, all other first-order Fourier components are equal to zero due to the superspace group symmetry conditions.

The i-$mC4(2)$ structure with first-order satellite reflections gives a reasonable fit to the diffraction pattern at this pressure. However, there are a small number of weak reflections that are not accounted for, the most intense of which are highlighted in Fig. 2(b). In order to test if these arise from higher-order satellite reflections, we collected a single exposure of our sample at ID09a following pressure cycling, as described previously. A Rietveld refinement of the i-$mC4(2)$ structure to this single pattern at 40.3 GPa is shown in Fig. 3(a), where satellite reflections up to third order have now been considered. The inclusion of second- and third-order satellite reflections results in an improved fit ($R_p = 5.6\%$ and $R_{wp} = 8.9\%$) in comparison with a refinement in which only first-order satellite reflections are considered ($R_p = 6.5\%$ and $R_{wp} = 10.3\%$). A larger number of second-order satellite reflections (≈12) are observed in this pattern, as well as a number of third-order satellite reflections, as illustrated in Fig. 3(b). Crucially, this structure can also explain a number of extremely weak satellite reflections at low angles, as illustrated in Fig. 3(c), which were not observed in the original data collected at I15 and which were therefore not used in the determination of the i-$mC4(2)$ structure model. The parameters of our final solution for the i-$mC4(2)$ structure at 40.3 GPa are $a = 2.9886(3)$ Å, $b = 5.2987(3)$ Å, $c = 4.5720$ Å, $\beta' = 90.328(8)^\circ$, and $y = 0.3365(9)$, with a modulation vector of [0.5863(3),0,1.5865(2)]. The refined modulation amplitudes are $B_{1a} = 0.042(5)$, $A_{1b} = -0.0363(2)$, $B_{1c} = 0.0693(19)$, $B_{2a} = -0.035(6)$, $A_{2b} = -0.008(3)$, $B_{2c} = 0.019(3)$, $B_{3a} = 0.018(11)$, $A_{3b} = -0.008(4)$, and $B_{3c} = 0.004(4)$. We

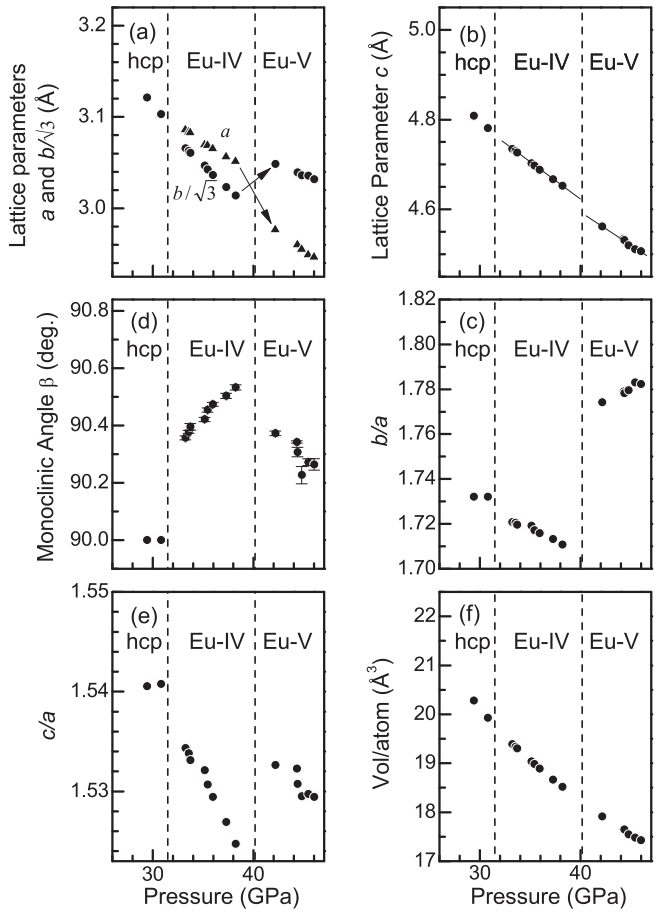

FIG. 4. Lattice parameters of Eu as a function of pressure, across the transition from hcp to i-$mC4$ (Eu-IV) and then to i-$mC4(2)$ (Eu-V). The hcp structure is described in the orthohexagonal setting, where the b/a axial ratio is equal to $\sqrt{3}$. For this reason, the pressure dependence of a (solid triangles) and $b/\sqrt{3}$ (solid circles) are both shown in (a), in order to illustrate the distortion of the structure from hcp. The arrows in (a) and the lines in (b) are added as guides to the eye. The lattice parameters were obtained from Rietveld fits to the diffraction profiles. With the exception of the monoclinic angle β, the error bars are smaller than the symbol size and so have been omitted.

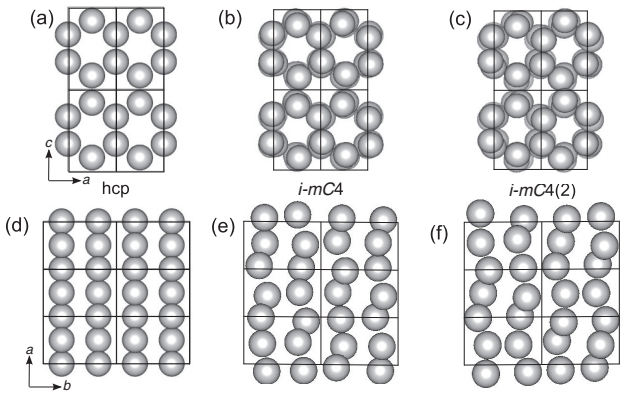

FIG. 5. Schematic views of the hcp, i-$mC4$ (Eu-IV), and i-$mc4(2)$ (Eu-V) structures at <31.5, 38, and 41 GPa, respectively. Four unit cells viewed along the b direction of the (a) hcp, (b) i-$mC4$, and (c) i-$mC4(2)$ structures, and six unit cells viewed along the c direction of the (d) hcp, (e) i-$mC4$, and (f) i-$mC4(2)$ structures. The modulation amplitudes are drawn to scale.

therefore conclude that Eu undergoes a transition to a second incommensurately modulated crystal structure at 38 GPa.

The i-$mC4(2)$ structure gives an excellent fit to the diffraction patterns collected up to 46 GPa, the highest pressure reached with this sample, when up to second-order satellite reflections are considered. Although this is an insufficient number of data points in order to be able to comment on the pressure dependence of the structural parameters of i-$mC4(2)$, we can consider the changes in the structural parameters of Eu across the transition from hcp to i-$mC4$ and then to i-$mC4(2)$. The pressure dependencies of the lattice parameters (a, $b/\sqrt{3}$, c, c/a, b/a, and volume/atom) are shown in Fig. 4. The hcp structure is described in the orthohexagonal setting, where the b/a axial ratio is equal to $\sqrt{3}$. For this reason, the pressure dependence of a and $b/\sqrt{3}$ are shown in the same panel for comparison. Discontinuities were observed in the c/a and b/a axial ratios, and also in the monoclinic angle β, across the transition from i-$mC4$ to i-$mC4(2)$. In particular, the b/a ratio was observed to decrease away from $\sqrt{3}$ following the transition to i-$mC4$, and then increase away from $\sqrt{3}$ following the transition to i-$mC4(2)$. The wave vector components also show discontinuous jumps across the transition from i-$mC4$ to i-$mC4(2)$, with q_1 going from $\sim$0.77 to $\sim$0.59, and q_3 going from $\sim$0.59 to $\sim$1.59. We therefore conclude that the transition is first order, with discontinuous changes in the structural parameters of the average structure, and also a rotation of the wave vector in the a-c plane.

This is the first incommensurate-incommensurate transition to be observed in a non-host-guest structure in the elements at high pressure. Schematic views of the hcp, i-$mC4$, and i-$mC4(2)$ structures along the b and c axes are shown in Fig. 5 for comparison, where the modulation amplitudes are drawn to scale.

Having solved the structure of Eu-V, we could then revisit the data collected in our initial studies. Only one single-phase Eu-V pattern was collected from the original sample loaded without a PTM, and the i-$mC4(2)$ structure gives an excellent fit to this pattern when up to $m = \pm 2$ satellite reflections were considered. Data from the sample loaded with a He PTM were collected up to much higher pressures, reaching a maximum pressure of 70.1 GPa. However, the patterns collected from this sample contained contaminant reflections from at least one additional impurity phase in addition to those from the $cI12$ impurity phase described in Ref. [8].

The i-$mC4(2)$ structure gives a good fit to the patterns collected below $\sim$50 GPa. However, this structure has six refinable lattice parameters (a, b, c, β, q_1, q_3), and so accurate peak positions of at least seven reflections are required in order to determine the unit cell dimensions and modulation vector. The diffraction profiles from this phase are very complex, with a large number of closely spaced reflections, and very high-resolution data are required in order to resolve individual peaks. Despite the use of a helium pressure medium, significant broadening of the sample reflections above $\sim$40 GPa made it increasingly difficult to determine accurate unit cell dimensions. This is illustrated in Fig. 6, which shows diffraction

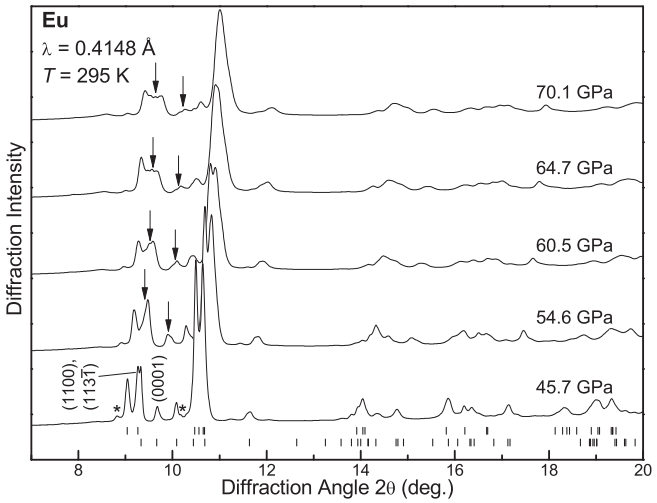

FIG. 6. (a) X-ray powder diffraction profiles of Eu at 45.7, 54.6, 60.5, 64.7, and 70.1 GPa collected from a sample loaded with a He PTM. The tick marks below the 45.7 GPa profile show the calculated peak positions of the main (upper) and first-order satellite (lower) reflections, as determined from a Rietveld refinement of the *i*-*mC*4(2) structure to this profile. The asterisks above the 45.7 GPa pattern indicate contaminant reflections from the *cI*12 contaminant phase. The arrows indicate the splitting of the (0001) reflection into a doublet, and the simultaneous change in the relative intensity of the (1100) and (113$\bar{1}$) reflections, with increasing pressure. The splitting of the (0001) reflection cannot be described by the *i*-*mC*4(2) structure.

profiles of Eu collected at 45.7, 54.6, 60.5, 64.7, and 70.1 GPa. The overall shape of the diffraction patterns are similar, and no dramatic changes are observed. However, taking into account the fact that the transition from Eu-IV to Eu-V is relatively subtle, and the overall diffraction patterns of both phases are also relatively similar, means that the possibility of similar transitions occurring at higher pressures cannot be ruled out. We note that in the patterns collected above 47.1 GPa, the (0001) satellite reflection appears to split into a doublet, with the splitting increasing at higher pressures, as highlighted in Fig. 6. This splitting cannot be accounted for by the *i*-*mC*4(2) structure when up to third-order satellites are considered. As said, the patterns from this sample contain reflections from at least one additional contaminant phase that has not been reported in previous studies, and so we cannot rule out the possibility that the apparent splitting is actually due to a contaminant reflection with a similar *d* spacing to the (0001) sample reflection. However, we simultaneously observe a change in the relative intensity of the (1100) and (113$\bar{1}$) reflections, which are also highlighted in Fig. 6. Taken together, there is thus evidence of a further structural change above 47.1 GPa, but higher resolution data are required to be more certain.

Higher pressure diffraction data on Eu were collected up to 92 GPa in the previous study by Bi *et al.* [5]. Their structural assignments are not consistent with our own data collected above 18 GPa. We note that they reported a transition from a mixed-phase region to a single-phase orthorhombic phase above 66 GPa, and so we would expect the diffraction patterns to simplify at this transition. We saw no clear evidence of any transitions in our own data, but it is possible that this transition may occur at slightly higher pressures than were reached in our studies.

Eu has been predicted to transform to a fully trivalent state at pressures of 15.5(15) or 35 GPa [20,21]. However, although initial spectroscopic studies reported Eu to undergo a continuous transition to a mixed-valence state on compression [22,23], a more recent study reported Eu to remain almost divalent up to 87 GPa [24]. Ytterbium (Yb), which is also divalent at ambient pressure, transforms to a hexagonal structure (*hP*3) at 98(5) GPa [25]. This structure is also observed in neodymium and samarium at high pressure [26], and its observation in Yb was cited as evidence of a transformation to a fully trivalent state above this pressure [25]. No evidence of any of the crystal structures that have been observed in the trivalent lanthanides at high pressures were observed in our own studies of Eu, supporting the idea that Eu has not become trivalent by ∼70 GPa.

Despite the unusual complex structures that have been observed in Eu at high pressure, it is one of the few remaining elements about which nothing is known beyond 100 GPa. But, unless it transforms to a higher-symmetry structure at higher pressures, the determination of the structural behavior at pressure exceeding ∼50 GPa will be extremely challenging due to the complexity of the diffraction patterns and the increasing broadness of the diffraction peaks. Extremely high-resolution diffraction data collected on noncontaminated samples will be required for further investigations in order to determine the structural behavior of Eu at megabar pressures.

B. High temperature studies

In order to investigate the temperature dependence of the incommensurate phases, high-temperature powder x-ray diffraction data were collected on two Eu samples on beamline I15, and additional data from one of these samples were collected on beamline ID09a. In these experiments, the pressure of the sample was increased at constant temperature with the aim of determining the position of the high-temperature phase boundaries, in particular that between the hcp and incommensurate phases. The majority of the data were collected at three different temperatures: 363, 428, and 449 K. The 363 and 428 K data were each collected during a single run, and the 449 K data were collected in one run from each of the two samples.

The results of our high-temperature studies are summarized in Fig. 7. The bcc–hcp transition, which is known to occur at 12.5 GPa at ambient temperature, was determined to occur between 11.1 and 13.6 GPa at 449 K. We can therefore tentatively suggest that the bcc–hcp phase boundary is close to vertical. The hcp–Eu-IV transition, which occurs at 31.5 GPa at ambient pressure, was determined to occur between 32.4 and 36.4 GPa at 363 K, and between 39.8 and 41.3 GPa at 428 K. This suggests that the pressure range over which the hcp phase is stable increases with increasing temperature.

At 363 K, the transition from Eu-IV to Eu-V was observed between 39.8 and 41.3 GPa at 313 K, which is again a slightly higher pressure than we observed at room temperature, where the transition was observed to start between 38 and 39 GPa. The Eu-IV–Eu-V phase boundary was also crossed at 428 K.

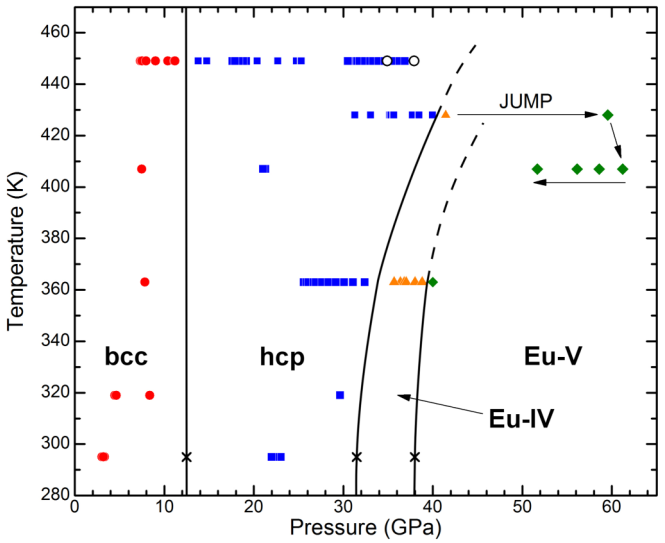

FIG. 7. (Color online) Phase diagram of Eu to 449 K. The (red) circles show the points in the bcc phase, the (blue) squares show the points in the hcp phase, the (orange) triangles show the points in the Eu-IV phase, and the (green) diamonds show the points in the Eu-V phase. The crosses show the room-temperature transition pressures, and the open circles show the points at which diamond failure occurred. The solid lines show an estimate of the phase boundaries, and the dotted lines show an extrapolation to higher temperatures. The data were collected on compression at constant temperature, with the exception of the data collected on Eu-V at 407 K, as indicated by the arrows.

However, the pressure of the sample jumped from 41.4 GPa in the Eu-IV phase to 59.5 GPa in the Eu-V phase (see Fig. 7), and so we were unable to determine the transition pressure at this temperature. However, this does confirm that both incommensurate phases are stable up to at least 428 K.

An attempt was made to cross the hcp–incommensurate phase boundary at 449 K in both of our samples. However, somewhat surprisingly, in both cases gasket failure leading to diamond failure was observed before we observed the transition to the incommensurate phase. The highest pressure hcp patterns were collected at 34.9 and 37.9 GPa, respectively, in the two samples.

There has been only one study of the high-pressure, high-temperature behavior of Eu, in which the melting curve was determined, although only to 7 GPa [27], and large areas of the phase diagram of Eu remain completely unknown. In the small pressure range in which the melting curve is known, a maximum was observed in the melting temperature of the bcc phase at about 3.5 GPa and 722 K. Similar behavior is observed in divalent Ba, which also exhibits a maximum in its melting temperature in the bcc phase [28]. At higher pressures, Ba exhibits a deep minimum in the melting curve at 7.7 GPa, close to the bcc–hcp transition. Given the similarities in their electronic structure, it is possible that this unusual melting behavior is also present in Eu. We note that in our previous high-pressure high-temperature experiments on K and Te, diamond failure was consistently observed in different sample runs on sample melting. In K, this was found to be due to a reaction between the sample and the Re gasket that occurred on sample melting [29]. Similar behavior was observed in Te on melting at ∼3 GPa and ∼750 K [30]. The fact that the diamonds failed at moderate pressures and temperatures in both of our Eu samples, and also that diamond failure was observed at very similar pressures and temperatures in each case (∼37 GPa, 449 K), suggests the possibility of a reaction between the Eu and the diamonds in this region of P-T space. This introduces the possibility of a minimum in the melting curve of Eu in this region of P-T space. Future studies using different gasket materials are required in order to investigate the behavior of Eu in this region.

IV. CONCLUSIONS

In summary, we have determined that Eu undergoes a transition from the incommensurately modulated Eu-IV to a second incommensurately modulated phase, Eu-V, above 38 GPa. Eu-IV and V have the same superspace group, but the modulation vectors differ in direction and magnitude. The transition involves discontinuous jumps in both the lattice parameters of the average structure and the wave vector components q_1 and q_3, and so we conclude that the transition is of first order. This is the first incommensurately modulated to incommensurately modulated transition to be observed in the elements at high pressure. Eu-V is stable to at least 46 GPa, and there is some evidence of another phase above that pressure. However, the sample reflections in the diffraction patterns collected above ∼50 GPa are very broad, and determining accurate structural details above this pressure will be very challenging. Despite these new results, Eu remains one of the few elements about which nothing is known above 100 GPa.

We have also performed high-pressure high-temperature studies up to 449 K in order to determine the position of the phase boundaries. The stability range of the hcp phase increases to higher pressures with increasing temperature. Further studies are required in order to determine the phase boundaries of the incommensurate Eu-IV and Eu-V phases in more detail.

ACKNOWLEDGMENTS

This work was supported by grants and a fellowship (I.L.) from the UK Engineering and Physical Sciences Research Council, and facilities were made available by the European Synchrotron Radiation Facility, Diamond Light Source, and the Research Complex at Harwell. Parts of this research were carried out at the light source PETRA III at DESY, a member of the Helmholtz Association (HGF). We thank M. Hanfland of ID09a (ESRF), and A. Kleppe and N. Casati of I15 (Diamond Light Source) for their assistance in using the beamlines, and U. Schwarz at the Max-Planck-Institut für Chemische Physik fester Stoffe in Dresden for providing the Eu samples. We would also like to thank S. MacLeod of AWE for the use of pressure cells and equipment, and we would like to acknowledge helpful discussions with Professor S. van Smaalen. M.I.M. and K.A.M. would like to thank AWE for the award of a William Penny Fellowship and a Case Studentship award, respectively, and R.J.H and E.E.M. would like to acknowledge financial support from EPSRC (UK) via the Scottish Doctoral Training Centre in Condensed Matter Physics.

[1] G. K. Samudrala and Y. K. Vohra, in *Handbook on the Physics and Chemistry of Rare Earths*, edited by J.-C. G. Bünzli and V. K. Pecharsky (North-Holland, Elsevier, Amsterdam, 2013), Vol. 43, Chap. 257, pp. 275–319.
[2] K. Takemura and K. Syassen, J. Phys. F: Met. Phys. **15**, 543 (1985).
[3] T. Krüger, B. Merkau, W. A. Grosshans, and W. B. Holzapfel, High Press. Res. **2**, 193 (1990).
[4] W. A. Grosshans and W. B. Holzapfel, Phys. Rev. B **45**, 5171 (1992).
[5] W. Bi, Y. Meng, R. S. Kumar, A. L. Cornelius, W. W. Tipton, R. G. Hennig, Y. Zhang, C. Chen, and J. S. Schilling, Phys. Rev. B **83**, 104106 (2011).
[6] R. J. Husband, I. Loa, G. W. Stinton, S. R. Evans, G. J. Ackland, and M. I. McMahon, J. Phys. Conf. Ser. **377**, 012030 (2012).
[7] R. J. Husband, I. Loa, G. W. Stinton, S. R. Evans, G. J. Ackland, and M. I. McMahon, Phys. Rev. Lett. **109**, 095503 (2012).
[8] R. J. Husband, I. Loa, G. W. Stinton, G. J. Ackland, and M. I. McMahon, High Press. Res. **33**, 158 (2013).
[9] H. K. Mao, J. Xu, and P. M. Bell, J. Geophys. Res. **91**, 4673 (1986).
[10] M. Hanfland (private communication).
[11] M. Hanfland, K. Syassen, and J. Köhler, J. Appl. Phys. **91**, 4143 (2002).
[12] P. I. Dorogokupets and A. R. Oganov, Phys. Rev. B **75**, 024115 (2007).
[13] A. P. Hammersley, ESRF Internal Report, ESRF97HA02T, "FIT2D: An Introduction and Overview" (1997).
[14] A. P. Hammersley, S. O. Svensson, M. Hanfland, A. N. Fitch, and D. Häusermann, High Press. Res. **14**, 235 (1996).
[15] A. Boultif and D. Louër, J. Appl. Crystallogr. **37**, 724 (2004).
[16] J. Rodrìguez-Carvajal, Physica (Amsterdam) B **192**, 55 (1993).
[17] V. Petříček, M. Dušek, and L. Palatinus, Z. Kristallogr. **229**, 345 (2014).
[18] S. van Smaalen, *Incommensurate Crystallography* (Oxford University Press, New York, 2007).
[19] C. Hejny and M. I. McMahon, Phys. Rev. Lett. **91**, 215502 (2003).
[20] B. Johansson and A. Rosengren, Phys. Rev. B **11**, 2836 (1975).
[21] A. Rosengren and B. Johansson, Phys. Rev. B **13**, 1468 (1976).
[22] J. Röhler, Physica B **144**, 27 (1986).
[23] R. D. Taylor and J. N. Farrell, J. Appl. Phys. **61**, 3669 (1987).
[24] W. Bi, N. M. Souza-Neto, D. Haskel, G. Fabbris, E. E. Alp, J. Zhao, R. G. Hennig, M. M. Abd-Elmeguid, Y. Meng, R. W. McCallum, K. Dennis, and J. S. Schilling, Phys. Rev. B **85**, 205134 (2012).
[25] G. N. Chesnut and Y. K. Vohra, Phys. Rev. Lett. **82**, 1712 (1999).
[26] Y. C. Zhao, F. Porsch, and W. B. Holzapfel, Phys. Rev. B **50**, 6603 (1994).
[27] Jayaraman, Phys. Rev. **135**, A1056 (1964).
[28] M. Winzenick and W. B. Holzapfel, Phys. Rev. B **55**, 101 (1997).
[29] O. Narygina, E. E. McBride, G. W. Stinton, and M. I. McMahon, Phys. Rev. B **84**, 054111 (2011).
[30] C. Hejny, S. Falconi, L. F. Lundegaard, and M. I. McMahon, Phys. Rev. B **74**, 174119 (2006).